Combined photoacoustic microscopy and optical coherence tomography can measure metabolic rate of oxygen

Tan Liu,[1] Qing Wei,[1] Jing Wang,[1] Shuliang Jiao,[2,3] and Hao F. Zhang[1,4]

[1]*Department of Biomedical Engineering, Northwestern University, Evanston IL 60208, USA*
[2]*Department of Ophthalmology, University of Southern California, Los Angeles, CA 90033, USA*
[3]*sjiao@usc.edu*
[4]*hfzhang@northwestern.edu*

Abstract: We proposed to measure the metabolic rate of oxygen (MRO_2) in small animals *in vivo* using a multimodal imaging system that combines laser-scanning optical-resolution photoacoustic microscopy (LSOR-PAM) and spectral-domain optical coherence tomography (SD-OCT). We first tested the capability of the multimodal system to measure flow rate in a phantom made of two capillary tubes of different diameters. We then demonstrated the capability of measuring MRO_2 by imaging two parallel vessels selected from the ear of a Swiss Webster mouse. The hemoglobin oxygen saturation (sO_2) and the vessel diameter were measured by the LSOR-PAM and the blood flow velocity was measured by the SD-OCT, from which blood flow rate and MRO_2 were further calculated. The measured blood flow rates in the two vessels agreed with each other.

OCIS codes: (110.5120) Photoacoustic imaging; (170.4500) Optical coherence tomography; (170.2655) Functional monitoring and imaging

References and links

1. L. Padnick-Silver, J. J. Kang Derwent, E. Giuliano, K. Narfström, and R. A. Linsenmeier, "Retinal oxygenation and oxygen metabolism in Abyssinian cats with a hereditary retinal degeneration," Invest. Ophthalmol. Vis. Sci. **47**(8), 3683–3689 (2006).
2. V. A. Alder, E. N. Su, D. Y. Yu, S. J. Cringle, and P. K. Yu, "Diabetic retinopathy: early functional changes," Clin. Exp. Pharmacol. Physiol. **24**(9-10), 785–788 (1997).
3. J. Stone, T. Chan-Ling, J. Pe'er, A. Itin, H. Gnessin, and E. Keshet, "Roles of vascular endothelial growth factor and astrocyte degeneration in the genesis of retinopathy of prematurity," Invest. Ophthalmol. Vis. Sci. **37**(2), 290–299 (1996).
4. R. C. deCharms, "Applications of real-time fMRI," Nat. Rev. Neurosci. **9**(9), 720–729 (2008).
5. N. Zhang, X. H. Zhu, Y. Zhang, J. K. Park, and W. Chen, "High-resolution fMRI mapping of ocular dominance layers in cat lateral geniculate nucleus," Neuroimage **50**(4), 1456–1463 (2010).
6. S. H. Hardarson, A. Harris, R. A. Karlsson, G. H. Halldorsson, L. Kagemann, E. Rechtman, G. M. Zoega, T. Eysteinsson, J. A. Benediktsson, A. Thorsteinsson, P. K. Jensen, J. Beach, and E. Stefánsson, "Automatic retinal oximetry," Invest. Ophthalmol. Vis. Sci. **47**(11), 5011–5016 (2006).
7. A. Harris, R. B. Dinn, L. Kagemann, and E. Rechtman, "A review of methods for human retinal oximetry," Ophthalmic Surg. Lasers Imaging **34**(2), 152–164 (2003).
8. H. Wehbe, M. Ruggeri, S. Jiao, G. Gregori, C. A. Puliafito, and W. Zhao, "Automatic retinal blood flow calculation using spectral domain optical coherence tomography," Opt. Express **15**(23), 15193–15206 (2007).
9. M. Szkulmowski, A. Szkulmowska, T. Bajraszewski, A. Kowalczyk, and M. Wojtkowski, "Flow velocity estimation using joint Spectral and Time domain Optical Coherence Tomography," Opt. Express **16**(9), 6008–6025 (2008).
10. Y. K. Tao, K. M. Kennedy, and J. A. Izatt, "Velocity-resolved 3D retinal microvessel imaging using single-pass flow imaging spectral domain optical coherence tomography," Opt. Express **17**(5), 4177–4188 (2009).
11. Z. Zhi, W. Cepurna, E. Johnson, T. Shen, J. Morrison, and R. K. Wang, "Volumetric and quantitative imaging of retinal blood flow in rats with optical microangiography," Biomed. Opt. Express **2**(3), 579–591 (2011).
12. Y. Wang, B. A. Bower, J. A. Izatt, O. Tan, and D. Huang, "*In vivo* total retinal blood flow measurement by Fourier domain Doppler optical coherence tomography," J. Biomed. Opt. **12**(4), 041215 (2007).
13. H. F. Zhang, K. Maslov, G. Stoica, and L. V. Wang, "Functional photoacoustic microscopy for high-resolution and noninvasive in vivo imaging," Nat. Biotechnol. **24**(7), 848–851 (2006).
14. H. F. Zhang, K. Maslov, and L. V. Wang, "*In vivo* imaging of subcutaneous structures using functional photoacoustic microscopy," Nat. Protoc. **2**(4), 797–804 (2007).

#143327 - $15.00 USD Received 28 Feb 2011; accepted 22 Apr 2011; published 27 Apr 2011

15. H. F. Zhang, K. Maslov, M. Sivaramakrishnan, G. Stoica, and L. V. Wang, "Imaging of hemoglobin oxygen saturation variations in single vessels *in vivo* using photoacoustic microscopy," Appl. Phys. Lett. **90**(5), 053901 (2007).
16. Z. X. Xie, S. L. Jiao, H. F. Zhang, and C. A. Puliafito, "Laser-scanning optical-resolution photoacoustic microscopy," Opt. Lett. **34**(12), 1771–1773 (2009).
17. S. L. Jiao, Z. X. Xie, H. F. Zhang, and C. A. Puliafito, "Simultaneous multimodal imaging with integrated photoacoustic microscopy and optical coherence tomography," Opt. Lett. **34**(19), 2961–2963 (2009).
18. H. F. Zhang, J. Wang, Q. Wei, T. Liu, S. Jiao, and C. A. Puliafito, "Collecting back-reflected photons in photoacoustic microscopy," Opt. Express **18**(2), 1278–1282 (2010).
19. A. Laugier and J. Garai, "Derivation of the Ideal Gas Law," J. Chem. Educ. **84**(11), 1832–1833 (2007).
20. H. Fang, K. Maslov, and L. V. Wang, "Photoacoustic Doppler effect from flowing small light-absorbing particles," Phys. Rev. Lett. **99**(18), 184501 (2007).
21. J. Yao and L. V. Wang, "Transverse flow imaging based on photoacoustic Doppler bandwidth broadening," J. Biomed. Opt. **15**(2), 021304 (2010).
22. R. M. Werkmeister, N. Dragostinoff, M. Pircher, E. Götzinger, C. K. Hitzenberger, R. A. Leitgeb, and L. Schmetterer, "Bidirectional Doppler Fourier-domain optical coherence tomography for measurement of absolute flow velocities in human retinal vessels," Opt. Lett. **33**(24), 2967–2969 (2008).
23. M. Sivaramakrishnan, K. Maslov, H. F. Zhang, G. Stoica, and L. V. Wang, "Limitations of quantitative photoacoustic measurements of blood oxygenation in small vessels," Phys. Med. Biol. **52**(5), 1349–1361 (2007).
24. E. W. Stein, K. Maslov, and L. V. Wang, "Noninvasive, *in vivo* imaging of blood-oxygenation dynamics within the mouse brain using photoacoustic microscopy," J. Biomed. Opt. **14**(2), 020502 (2009).
25. S. Jiao, M. Jiang, J. Hu, A. Fawzi, Q. Zhou, K. K. Shung, C. A. Puliafito, and H. F. Zhang, "Photoacoustic ophthalmoscopy for in vivo retinal imaging," Opt. Express **18**(4), 3967–3972 (2010).

1. Introduction

Studying microcirculation in the retina plays an important role in ophthalmic research. Because the retina is a highly energy-demanding tissue, an abnormal oxygen supply may lead to several vision disorders. For example, retinal degeneration [1], diabetic retinopathy [2] and retinopathy of prematurity [3] have been reported to be correlated with disrupted local retinal oxygen environments, which can be quantified by intraretinal oxygen distribution and metabolic rate of oxygen (MRO_2, also can be referred to oxygen consumption). Hence, a technology that is able to measure MRO_2 in the retina is desired. Such a technology should possess the following characteristics: (1) noninvasiveness; (2) label-free; (3) fast-acquisition; (4) high-spatial resolution, and (5) capable of measuring multiple functional parameters, such as hemoglobin oxygen saturation (sO_2) and blood flow; however, no existing technology satisfies all the above requirements.

Currently, measuring retinal MRO_2 primarily relies on oxygen-sensitive microelectrodes [1,2], which is not only invasive but also terminal. Blood-oxygen-level-dependent contrast MRI has also been used to measure ocular MRO_2; however, its spatial resolution is insufficient in microcirculation studies [4,5]. Fundus photography-based retinal oximetry has the potential to quantify sO_2 [6,7] and several optical coherence tomography (OCT) based technologies have been reported to measure retinal blood flow [8–12]; but each individual technology is insufficient to measure MRO_2 as both sO_2 and blood flow measurements are required.

Here, we demonstrate the feasibility of measuring MRO_2 at the microvascular level *in vivo* without extrinsic contrast agent using a combined laser-scanning optical-resolution photoacoustic microscopy (LSOR-PAM) and spectral-domain OCT (SD-OCT).

2. Methods and materials

To measure the MRO_2 *in vivo*, we selected an artery-vein pair and acquired the following parameters: the sO_2 in artery and vein (sO_{2a} and sO_{2v}, dimensionless), the mean total hemoglobin concentration ($\overline{\mathrm{HbT}}$, g/L) in blood, the diameters of the artery and vein (d_a and d_v, m), and the mean blood flow velocities in the artery and vein ($\overline{v}_a$ and $\overline{v}_v$, m/s). Assuming that vessels have circular cross-sections, total hemoglobin concentration is constant, and each hemoglobin molecule carries four oxygen molecules, the MRO_2 (g/min) is given by

#143327 - $15.00 USD Received 28 Feb 2011; accepted 22 Apr 2011; published 27 Apr 2011

$$\mathrm{MRO_2} = 60 \cdot \frac{4 \cdot \mathrm{W_{O2}}}{\mathrm{W_{HbO2}}} \cdot \left[[\overline{\mathrm{HbT}}] \cdot \mathrm{sO_{2a}} \cdot (\frac{\pi}{4} \cdot d_a^2) \cdot \overline{v}_a - [\overline{\mathrm{HbT}}] \cdot \mathrm{sO_{2v}} \cdot (\frac{\pi}{4} \cdot d_v^2) \cdot \overline{v}_v \right]$$
$$= \frac{60 \cdot \pi \cdot \mathrm{W_{O2}}}{\mathrm{W_{HbO2}}} \cdot [\overline{\mathrm{HbT}}] \cdot \left(\mathrm{sO_{2a}} \cdot d_a^2 \cdot \overline{v}_a - \mathrm{sO_{2v}} \cdot d_v^2 \cdot \overline{v}_v \right), \quad (1)$$

where W_{O2} and W_{HbO2} are the molecular weights of O_2 and oxy-hemoglobin, which are 32 and 68000, respectively.

In Eq. (1), the sO_2 was calculated based on multi-wavelength LSOR-PAM measurements [13–15]. The $\overline{\mathrm{HbT}}$ was measured from blood samples by a commercial veterinary laboratory. The diameters of the blood vessels were measured by LSOR-PAM along the lateral direction.

The mean blood flow velocity was measured by the SD-OCT based on [8]

$$\overline{v} = \frac{f_{\mathrm{sample}} \cdot \lambda_0 \cdot \Delta\phi}{4 \cdot \pi \cdot n \cdot \cos\theta} \quad (2)$$

where f_{sample} is the A-line rate; λ_0 is the central wavelength of the probing light; n is the refractive index of sample (~1.4 for soft tissue and ~1.33 for water); $\Delta\varphi$ is the unwrapped phase shift between adjacent A-lines which ranged in [-π, + π]; and θ is the OCT Doppler angle (the angle between incident probing light and the blood vessel flow direction).

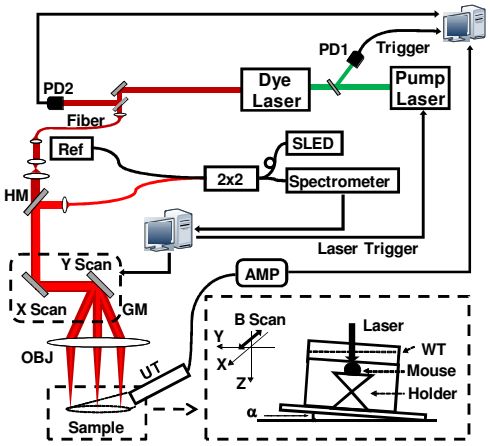

Fig. 1. Schematics of the combined LSOR-PAM and SD-OCT. PD: photodiode; 2 × 2: 2 × 2 single-mode optical fiber coupler; HM: hot mirror; GM: 2D galvanometer; OBJ: objective lens; AMP: amplifier; UT: ultrasonic transducer; WT: water tank; SLED: superluminescent emitting diode; Ref: OCT reference arm.

The schematic of the integrated LSOR-PAM and SD-OCT is shown in Fig. 1. The optical illumination and ultrasonic detection in the LSOR-PAM have been described elsewhere [16,17]. To brief, we used a tunable dye laser (Cobra, Sirah Laser and Plasmatchnik GmbH) pumped by a Nd:YLF laser (IS8II-E, Edge-Wave GmbH; pulse duration: 6 ns; repetition rate: 1024 Hz) as the irradiation source. The dye laser output was coupled into a single mode optical fiber and was then merged with the OCT probing light by a dichroic mirror (NT43-955, Edmund Optics). The combined beams were scanned by an x–y galvanometer (6230H, Cambridge Technology) and were focused by an achromatic lens with 40-mm focal length (AC254-040-A1, Thorlabs). We used four optical wavelengths (570 nm, 578 nm, 588 nm, and 590 nm) in the multiwavelength measurement for sO_2.

A custom-built unfocused needle ultrasonic transducer (center frequency: 35 MHz; bandwidth: 50%; active element size: 0.5 × 0.5 mm^2) was used to detect the PA waves. The detected PA signals were amplified by 49 dB and were digitized by a high speed digitizer (CS 14200, Gage Applied) at a sampling rate of 200 MS/s. The energy of each laser pulse was

#143327 - $15.00 USD Received 28 Feb 2011; accepted 22 Apr 2011; published 27 Apr 2011

sampled by the photodiode PD2 (DET10A, Thorlabs) to compensate for the pulse energy instability. As reported in our previous work, the lateral resolution of the LSOR-PAM is 2.8 μm, and the axial resolution is 23 μm [18].

The SD-OCT system used a broadband superluminescent emitting diode (SLED) as the light source (IPSDD0804, InPhenix; center wavelength λ_0: 840 nm; 3-dB bandwidth $\Delta\lambda$: 50 nm). The output light was coupled into a 2 × 2 single-mode optical fiber coupler after being attenuated by 3 dB. A home-made spectrometer was used to detect the interference light with an A-line rate (f_{sample}) of 24 kHz. The axial resolution is 6 μm in tissue and the lateral resolution is 20 μm [17]. In order to measure flow, the animal holder and the water tank were both tilted by an angle (quantified in the acquired 3D OCT images) as shown in Fig. 1.

A flow phantom was made of two polystyrene capillary tubes (CTPS125-250-5 and CTPS250-500-5, Paradigmoptics; inner diameters: 125 μm and 250 μm; outer diameters: 250 μm and 500 μm). The two tubes were glued interconnected and the thinner tube was connected to a perfusion pump (A-99, Razel) for flow control. As a result, the two tubes have identical flow rate but different flow velocity. Diluted red ink (10%) mixed with 1% Intralipid solution was used to mimic blood. The two tubes were placed in parallel at the bottom of the water tank and were tilted by 5.6° with respect to the OCT probing light.

In the *in vivo* experiment, a Swiss Webster mouse (Harlan Co.; body weight: 20 g) ear was imaged. The animal was anesthetized by a mixture of 1.5% isoflurane and regular air. After hairs were removed by a commercial nonirritating hair-removing lotion, the animal was fixed on a homemade animal holder during the imaging period. The mouse ear was placed on a flat supporter and the supporter was tilted by 3.8° with respect to the OCT probing light. The mouse was sacrificed after data acquisition and blood samples were taken for $\overline{\text{HbT}}$ measurement. All experimental animal procedures conformed to the laboratory animal protocol approved by the Animal Care and Use Committee of the University of Wisconsin–Milwaukee, where the experiments were conducted.

3. Results and discussions

3.1. Flow phantom results

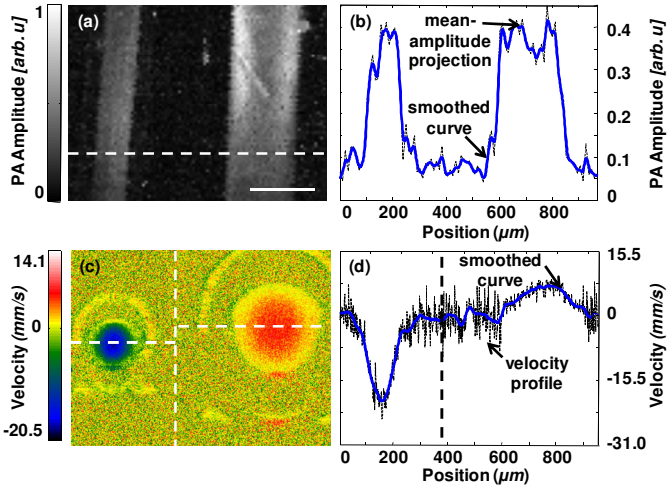

Fig. 2. Flow phantom imaging results. (a) LSOR-PAM image of the tubes (mean intensity projection); (b) PA amplitude profile along the dashed line in panel a; (c) flow velocity measured by Doppler OCT at the cross section marked in panel a; (d) the flow velocity profile at locations marked by the two dash lines in panel c. Bar: 250 μm.

Figure 2 shows the phantom imaging results. Figure 2a is the LSOR-PAM mean-amplitude-projection image of the capillary tubes acquired at the optical wavelength of 570

#143327 - $15.00 USD Received 28 Feb 2011; accepted 22 Apr 2011; published 27 Apr 2011

nm. The angles between the center lines of the tubes with respect to the vertical axis of the image are measured to be 4.8° (left) and 2.4° (right), which were used to correct the measured tube diameters. Figure 2b shows the PA amplitude (averaged for 32 times) along the dashed line in Fig. 2a and the tube diameter were measured to be d_1 = 134.46 ± 0.98 μm (left) and d_2 = 249.83 ± 0.39 μm (right). Figure 2c shows the Doppler OCT result measured at the location marked in Fig. 2a. The Doppler angle was 84.4° and the calculated mean flow velocities were $\overline{v}_1$ = −11.20 ± 0.32 mm/s and $\overline{v}_2$ = 3.40 ± 0.37 mm/s. The sign of the velocity represents the flow direction.

We compared the flow rates $F = 60 \cdot \pi \cdot d^2 \cdot \left|\overline{v}\right| / 4$ between the two capillary tubes. The pump was set at flow rate of 0.595 cc/hr (9.92 μl/min); and we calculated that F_1 = 9.51 ± 0.14 μl/min and F_2 = 9.94 ± 1.12 μl/min. The comparable flow rates between the two capillary tubes demonstrated the self-consistency in the multimodal measurement, which also agreed with the pump value.

3.2. In vivo results

To test the feasibility of measuring MRO_2, the microvasculature in mouse ears was used as an analogue of retinal vessels because both objects are optically thin.

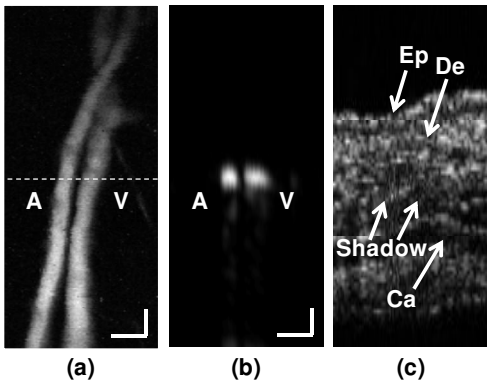

Fig. 3. Multimodal anatomic imaging of a mouse ear. (a) LSOR-PAM projection image of an artery-vein pair; (b) LSOR-PAM B-Scan image acquired at the 570-nm optical wavelength at the location marked by the dashed line in panel a; (c) OCT B-Scan image acquired at the same location. A: Artery; V: Vein; Ep, epidermis; De, dermis; Ca, cartilaginous backbone; Bar: 100 μm.

Figure 3 shows the *in vivo* anatomic images. The mean-amplitude-projection image of two parallel vessels (an artery-vein pair) is shown in Fig. 3a. The quantification of sO_2 and blood flow in these two vessels was performed in B-scan images at the location highlighted by the dashed line. Figure 3b shows the PAM B-scan image acquired at 570 nm after being averaged over 256 consecutive B-scans, where the two vessels are clearly dominating. Figure 3c shows the corresponding OCT B-scan image at the same location, where skin anatomy and the cartilage layer are visualized but not the blood vessels. However, the shadows created by the vessel pair can be observed.

Figure 4 shows the functional imaging results. The sO_2 values were calculated based on the B-scan images acquired at the four optical wavelengths after a 3 × 3 spatial averaging in each B-scan image and only the peak PA amplitudes of the two vessels were used. The measured sO_2 distinguished the artery (sO_{2a} = 68.9%) and vein (sO_{2v} = 38.3%) in the vessel pair (Fig. 4a). The vessel diameters were measured to be d_a = 42.69 ± 0.09 μm and d_v = 61.13 ± 0.25 μm using the method as we used in the flow phantom.

Figure 4b shows the Doppler OCT results. The angle between the surface of the mouse ear and the horizontal plane was 3.8°; hence, the Doppler angle was θ = 86.2°, which is

#143327 - $15.00 USD Received 28 Feb 2011; accepted 22 Apr 2011; published 27 Apr 2011

comparable with the reported Doppler angle in human eyes [8]. The mean velocities were $\overline{v}_a$ = −15.58 ± 0.43 mm/s and $\overline{v}_v$ = 8.11 ± 0.48 mm/s, as shown in Fig. 4b.

We compared the blood flow rate in this vessel pair. Using the measured blood flow velocities and diameters, we have F_a = 1.34 ± 0.04 μl/min and F_v = 1.43 ± 0.10 μl/min, which are comparable and, thus, shows that the measurements are self-consistent.

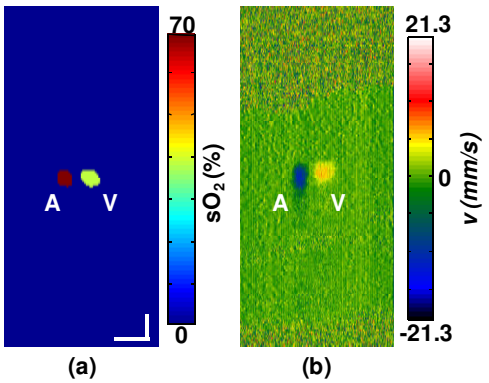

Fig. 4. Multimodal functional imaging. (a) Imaged sO_2 using LSOR-PAM; (b) Imaged blood flow velocity using SD-OCT. Bar: 100 μm.

Finally, based on the $\overline{\text{HbT}}$ value of 344 g/L, the MRO_2 was 242.77 ± 30.50 ng/min, assuming that the vessel pair supports the same tissue volume. We want to point out here that MRO_2 depends on the subject and the anatomic sites because sO_2 and blood flow vary significantly between subjects and anatomic locations.

We further converted the measured MRO_2 into a more commonly used unit of liter/min. The ideal gas law [19] calculates the volume of oxygen (gas) from its weight by

$$V = n_g RT / P \tag{3}$$

where n_g is the number of moles of gas, R is the molar gas constant 8.3145 J·mole^{-1}·K^{-1}, T is the blood temperature (311.15 K), and P is the standard atmosphere pressure (101,325 Pa). Based on the molar mass of oxygen (32 g/mol), the MRO_2 is 193.70 ± 24.33 nl/min.

In the current study, the blood flow velocity was measured by SD-OCT. Although transverse blood flow velocity can be measured by both amplitude-modulated continuous-wave and pulsed illuminating PAM [20,21], these methods require extra visible light exposure, which is not preferred in ophthalmic imaging. PAM also has the potential to measure $\overline{\text{HbT}}$ if one of the isosbestic optical wavelengths in the molar extinction coefficient spectra of the oxy- and deoxy-hemiglobin [15] is used and the correlation between the hemoglobin concentration and the measured PA amplitude is calibrated. However, such a capability has not been reported yet and, oftentimes, the calibration is not trivial in *in vivo* studies as the actual measured PA amplitude can be affected by local optical fluence and is strongly sample dependent. Taking blood sample is routine in many of the existing clinical diagnosis and, more important, it will be much more precise.

We need to address a few issues in the future. First, a higher SNR in the LSOR-PAM needs to be achieved. Since an unfocused rather than a strongly focused ultrasonic transducer is used to coordinate with the optical scanning for a much higher imaging speed, the SNR becomes worse and signal averaging is required to minimize the errors in sO_2 calculation. A weakly spherical focused ultrasonic transducer can potentially be employed. Second, the Doppler angle was introduced by tilting the sample in this study, which was hard to control in patient. A dual-beam OCT can potentially be used to avoid tilting the samples and still measures the absolute blood flow velocity [22].

#143327 - $15.00 USD Received 28 Feb 2011; accepted 22 Apr 2011; published 27 Apr 2011

No compensation for the wavelength-dependent fluence attenuation was conducted in this study. Although missing or poor optical fluence compensation leads to a noticeable measurement inaccuracy in deep tissue [23,24], it is unlikely to affect the application in ophthalmology [25] since the medium between cornea and retinal vessel (vitreous humor) is often considered transparent, inducing minimal attenuation of light within the visible and NIR spectral range.

4. Conclusion

In conclusion, we demonstrated the feasibility of measuring MRO_2 using a combined LSOR-PAM and SD-OCT multimodal system. The multimodal imaging system was first tested in a flow phantom. Then i*n vivo* measurement of MRO_2 was achieved in microvessels and the measured parameters by different modalities were self-consistent. This work lays the foundation for the next-stage retinal MRO_2 imaging, which has great potential in both fundamental study and clinical early diagnosis of several blinding diseases.

Acknowledgments

The authors thank Dr. Berri Forman, Mrs. Rebecca Krumnow and Mrs. Jennifer Nemke for blood sample collection. This work was supported in part by the NIH 1RC4EY021357, the NSF CAREER CBET-1055379, the Shaw Scientist Award, and the Juvenile Diabetes Research Foundation Innovative Grant No. 5-2009-489.